On Measuring Thermal Diffusivity of a Thin Foil: Photothermal Variations

Paolo Bison[a,#], Giovanni Ferrarini[a], Stefano Rossi[a]

a Construction Technologies Institute, National Research Council (CNR), Padova, Italy

 # Corresponding Author: paolo-bison@cnr.it

Abstract

Some analytical solutions of the heat conduction differential equation in 2D case are presented for the geometry of the *Thin Foil* with thickness so small that the temperature variation is negligible through it. The model is successively applied to some *Photothermal* experimental schemes to evaluate the thermal diffusivity of the material of the thin foil.

1. Modeling the pulse with gaussian distribution of energy

The idea of an *instantaneous point source of heat*, that is, of a finite quantity of heat instantaneously liberated at a given point and time in an infinite solid, has proved most useful in the theory of conduction of heat [1].

The differential equation of heat conduction

$$\frac{\partial^2 T}{\partial x^2}+\frac{\partial^2 T}{\partial y^2}+\frac{\partial^2 T}{\partial z^2}-\alpha\frac{\partial T}{\partial t}=0 \qquad (1)$$

is satisfied by the fundamental instantaneous point source solution [2] which was systematically used for the first time by William Thomson (lord Kelvin)

$$T(x,y,z,t)=\frac{Q}{\rho c_p}\frac{1}{\pi^{3/2}}\frac{1}{(4\alpha t)^{3/2}}e^{-\frac{x^2+y^2+z^2}{4\alpha t}} \qquad (2)$$

where x,y,z [m] are the space variables, t [s] is time, T [K] is temperature, $\alpha = \lambda/\rho\, c_p$ [$m^2\, s^{-1}$] is the thermal diffusivity, λ [$W\, m^{-1}\, K^{-1}$] the thermal conductivity, ρ [$kg\, m^{-3}$] the density and c_p [$J\, kg^{-1}\, K^{-1}$] the specific heat. Such solution tends to 0 as t -> 0 at all points except in x=0, y=0, z=0 where it becomes infinite.

Notwithstanding the usefulness of such basic solution, mainly as a genetic material to prepare other (more complex) solutions, primarily by convolution in space and time, it

is difficult to generate it within a solid and even more difficult to measure or visualize it. It is therefore interesting to reduce the number of space variable to x, y by making negligible the z. In this case it is easy to generate a point source (for example with a focused laser shot) and to visualize the temperature field (e.g. by an IR camera), without any perturbing contact with the system.

It is considered the solution of the heat conduction equation on the thin foil made of homogeneous and isotropic material. It lies on the z=0 plane, with thickness l [m] so small that the temperature variation over it is negligible. Being h [W m^{-2} K^{-1}] the heat exchange coefficient between the foil and the environment, the PDE is [1]

$$\frac{\partial^2 T}{\partial x^2} + \frac{\partial^2 T}{\partial y^2} - \alpha \frac{\partial T}{\partial t} - \nu T = 0 \qquad (3)$$

and the solution [1] for the instantaneous release of a point source in O(0,0) is:

$$T_\delta(x, y, t) = \frac{Q}{4\pi\lambda l t} e^{-\alpha\nu t} e^{-\frac{x^2+y^2}{4\alpha t}} \qquad (4)$$

where $\nu = 2h/\lambda l$ [m^{-2}] is the parameter depending on the heat exchange with the ambient and Q [J] is the energy released by the pulse at the origin.

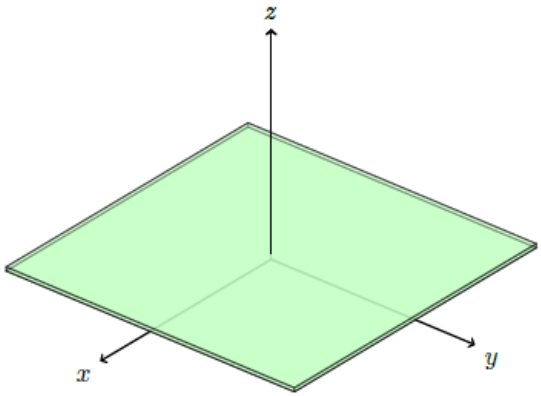

Figure 1. The thin foil

If the source is not a point but is distributed on the surface according to a prescribed function of the spatial coordinates, the solution can be obtained by spatial convolution

of Eq. 4 with the actual shape of the heating. The case of a laser beam with gaussian intensity profile [3], with diameter D_0 at 1/√e is easily computed:

$$T_G(x,y,t) = \frac{Q}{4\pi\lambda l t} e^{-\alpha\nu t} \int_{-\infty}^{\infty} d\xi \int_{-\infty}^{\infty} d\eta \frac{1}{\pi} \frac{1}{D_0^2/2} e^{-\frac{\xi^2+\eta^2}{D_0^2/2}} e^{-\frac{(x-\xi)^2+(y-\eta)^2}{4\alpha t}}$$

$$= \frac{Q}{\rho c_p l} e^{-\alpha\nu t} \frac{1}{\pi} \frac{1}{D_0^2/2+4\alpha t} e^{-\frac{x^2+y^2}{D_0^2/2+4\alpha t}} \qquad (5)$$

where the red color highlights the spatial gaussian distribution released on the surface. The solution is separable and integrating along x, y gives a constant value, independently from time. In this case, because the gaussian function is normalized, it is:

$$\frac{1}{\pi} \frac{1}{(D_0^2/2+4\alpha t)} \int_{-\infty}^{\infty} \int_{-\infty}^{\infty} e^{-\frac{x^2+y^2}{D_0^2/2+4\alpha t}} dx\, dy = 1 \qquad (6)$$

for each value of time t.

Hence, by integrating in x and y the temperature field, one obtains a function that decreases exponentially in time, with the time constant 1/αν:

$$\int_{-\infty}^{\infty} \int_{-\infty}^{\infty} T_G(x,y,t) dx\, dy = const \cdot e^{-\alpha\nu t} \qquad (7)$$

that can be used to evaluate the average heat exchange coefficient between the foil and the ambient, once the thermal diffusivity α has been estimated by the in-plane analysis, as shown by Cernuschi et al. [3].

2. Experimental lay-out

A foil of AISI T302, 500X150 mm, and 25 μm thickness is clamped on both 150 mm sides, by two aluminum bars, tightened with 4 bolts and nuts. The foil is suspended vertically by suitable handles. A pulsed laser source is used to heat one side of the foil. The energy released by the laser is ~ 1 J. The pulse duration is 1 ms. The beam has a diameter of 1'' and it is focused by a lens on the back side of the foil. The diameter of the focused beam (assuming it being distributed as a gaussian function) is ~ 1 mm at 1/e. On the other side of the foil, the IR camera (FLIR X6981 SLS LW [7.5 – 12.0μm], 640 X 512 pixels, frame rate

1 kHz) collects a sequence of images, in correspondence of the laser shot. The camera is equipped with a microscope lens 1:1, that means the field of view of each pixel is equal to the pitch of the detector, i.e. 25X25 μm. The experimental lay-out is shown in Fig. 2.

3. Experiments

3.1 The foil coated with graphite

The foil was coated with graphite Graphit 33, on the heated side to increase the absorptivity coefficient, and, on the camera side, to increase the emissivity.

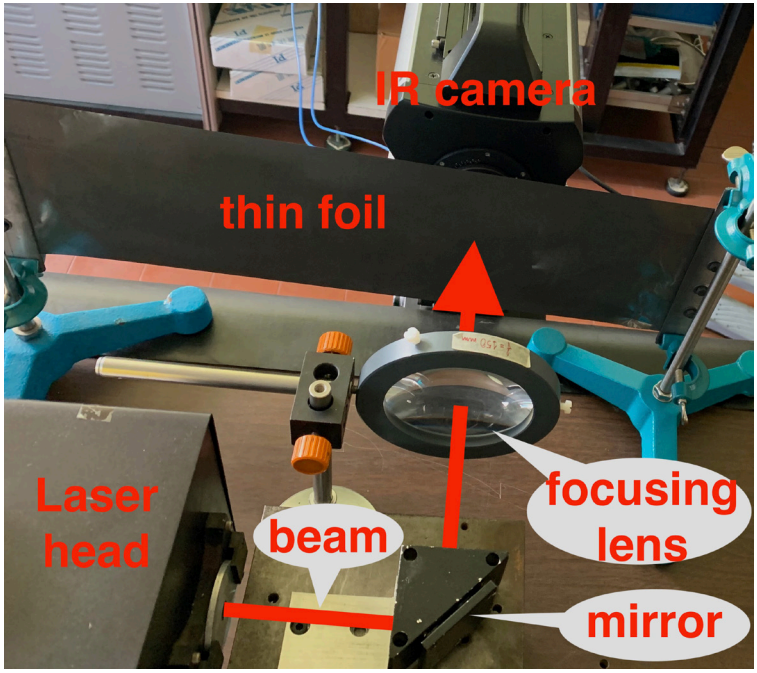

Figure 2. Experimental lay out

The laser shots one pulse and the camera collects 100 images (100 ms) before the shot and 500 images (500 ms) after the shot. The images before the shot are averaged and subtracted to the images during and after the shot. The temperature plot, measured on the camera side of the foil, in correspondence of the center of the gaussian heating and at 750 μm and 1250 μm far from the center, are shown in Fig. 3.

3.2 The foil without the graphite coating

The graphite coating could false the correct measurement of the in-plane thermal diffusivity. Indeed, the layers of graphite, sprayed on both sides of the foil, even though very thin, could increase the overall thermal conduction of the foil. To verify if it could affect the final result, the graphite coating was eliminated from both sides of the foil. Evidently, the measurement is becoming more difficult. On one side (the laser side), the energy absorbed decreases due to the low absorptivity of the foil (it is by eyes almost a mirror). On the other side (the camera side), the emissivity is very low, and the apparent thermographic signal is poor. As a result, the signal to noise ratio (S/N) is unacceptable. The S/N could be improved by statistical analysis of many experiments carried on at the same conditions. The experiments can be successively averaged. The signal is expected to emerge from the noise that, if randomly distributed, should decrease as the square root of the number of the experiments. On this purpose, the laser system is configured to deliver periodically a shot with duration 1 ms and energy 1 J. The period between two successive shots is 1 s. In correspondence of each shot the laser system sends a trigger to the IR camera system that starts the acquisition of 50 images at a frame rate of 1 kHz, that is for 50 ms after each shot.

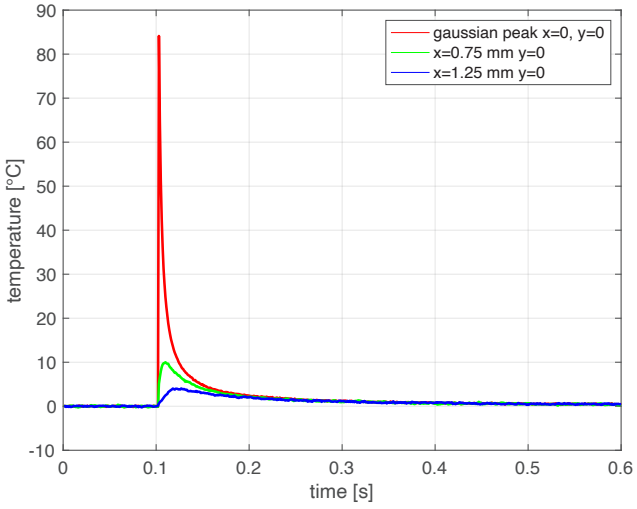

Figure 3. Temperature plot in correspondence of the center of the gaussian distribution of heat and far from the center at 0.75 mm and 1.25 mm respectively. Notice the maximum of temperature moving forward in time when spatially moving far from the center of the gaussian distribution.

An unexpected phenomenon appeared during the test without graphite coating. As expected, the temperatures in the image appear largely negative (see Fig. 4). This is due to the poor emissivity and consequently to the large reflectivity. Therefore, the temperature the camera collects is that of its cooled detector that is mirrored by the foil. It is known as the 'Narcissus' effect. The unexpected phenomenon is the apparent decrease of temperature, in phase with the laser shot, far from the supposed heated zone. Fig. 5 shows on the left a sequence of 20 shots at a frequency of 1 Hz. On the right a blow-up of three shots. It is apparent the decrease of the temperature in a zone not affected by the shot (3.3 mm far from the spot). The reason can be found considering the thermal expansion that is well known and exploited in the pump and probe photothermal/photoacoustics techniques [4]. The thermal expansion distorts the viewing angles of some parts of the foil. The highly directional reflectivity changes the apparent cold zones periodically, in phase with the shot. Due to this effect, that makes impossible a reliable fit of the temperature field, it was decided to paint with graphite the thin foil side facing the IR camera. The one facing the laser beam was left unpainted. Evidently, the thermal expansion is still present, but the apparent variation of temperature is cancelled, because the reflectivity becomes negligible and the graphite owns an emissivity that is not dependent from the angle of view (Lambertian emission).

4. Data reduction

In the following sections the processing of data is described.

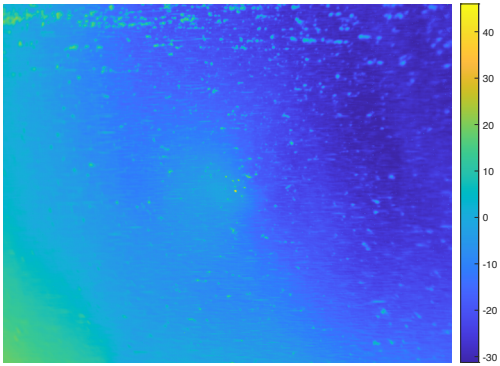

Figure 4. Without graphite coating, the surface reflects the temperature of the camera detector that is 67 K. For this reason, the temperature appears largely negative. This is known as the 'Narcissus' effect. In the center of the image, the laser spot barely appears.

4.1 With graphite coatings

Each sequence is treated in the following way:

1. The 100 pre-trigger images are averaged pixel by pixel along time. The resulted image is subtracted, pixel by pixel to any other image in the post-trigger sequence. As a result, the signal of the post-trigger images starts from around zero. Moreover, the IR images appear less affected by localized non-uniformities due to the emissivity variations. See Fig. 6.
2. The post-trigger sequence is considered: the imprint of the gaussian shot emerges from the background immediately after the shot due to the negligible thickness of the foil. See Fig. 7
3. Each post-trigger image is fitted with a 2D gaussian function. Among the estimated parameters, the most important is the denominator of the argument of the exponential function, that is increasing in time, from its initial value $D_0^2/2$, with a 2 slope equal to 4α. See Fig. 8.

4.2 Results with graphite

Total number of tests was 136. The results are reported in Fig. 9. Some outliers can be noticed that correspond to a poor laser shot. Indeed the lamp voltage is tuned to a very low value that is at the limit of laser ignition. Nonetheless a mean value of thermal diffusivity around $1.66 \cdot 10^{-5}$ is quite evident.

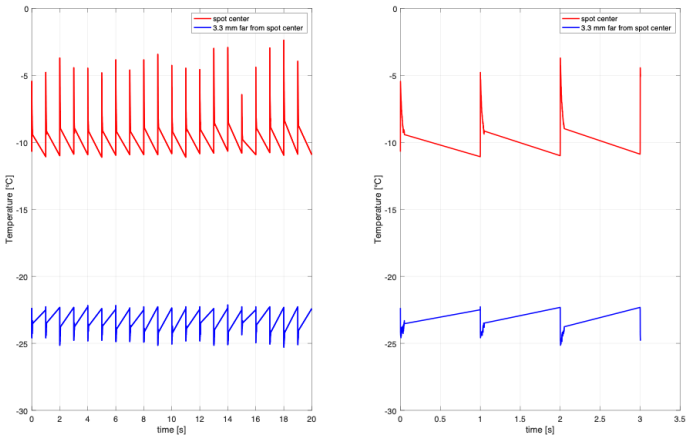

Figure 5. On the left a sequence of 20 shots. On the right the blow up of the plot that shows better the increase of temperature in correspondence of the shot (red curve) and the corresponding decrease of temperature far from the shot (blue curve). Data are collected for 50 ms after the trigger. The first image (datum) is at ambient temperature. The second image shows the shot. From 50 ms till the successive trigger (shot), 1 s later, no data are collected. This explains the straight line that connects the last datum of every periodic grabbing with the successive one.

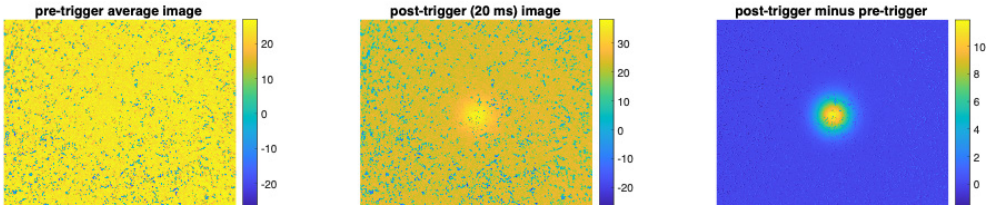

Figure 6. On the left the averaged image of the pre-trigger buffer. On the center the image taken 20 ms after the laser shot. On the right, the former minus the latter. The image on the right is an improved version of the center image, because the structural noise due to the emissivity variation was partially cancelled by the subtraction with the pre-trigger image.

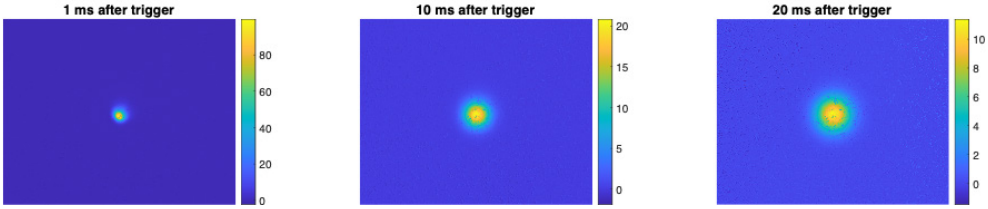

Figure 7. The temperature maps showing the gaussian distribution of heat are shown at the moment of the shot and at successive times. Notice the spreading of the distribution and the decrease of its maximum value (see the scale on the left of each image).

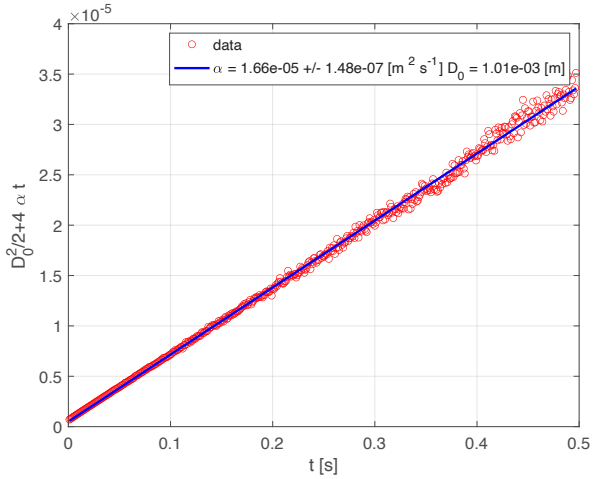

Figure 8. Plot of the diameter of the gaussian function that fit at best the temperature data. The fitting is applied to each image in the post-trigger sequence. The diameter is increasing in time as shown by the red dots. The slope of the straight line, fitting the red dots, gives the in-plane thermal diffusivity. In this case the pixel calibration is necessary to obtain the thermal diffusivity. Thanks to the 1:1 optics that is mounted on the IR camera, the pixel dimension is known to be the

pitch of the matrix detector, that is 25 µm. The diameter D_o at t = 0 s is related to the intercept of the line with the y axis.

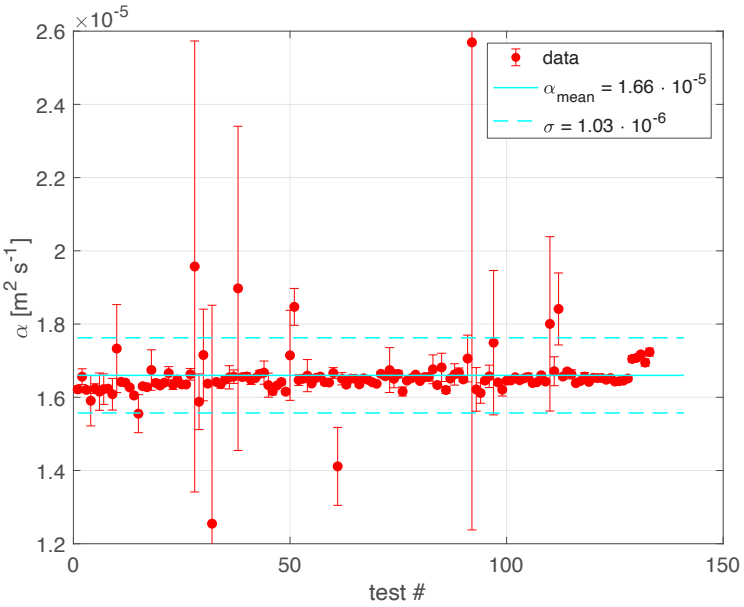

Figure 9. Plot of the results of 136 tests. The errorbar for the singular test is generally lower than the global errorbar that can be inferred by repeating the test. Evidently, the non-controlled parameters that affect the measurements (e.g. the energy of laser that is not stable) affect the results.

4.3 Without graphite coatings

Each sequence is treated in the following way:

4. A first run is done without any laser shot. This needs to eliminate a small drift due the intermittent (periodic) working time of the camera that does not reach the steady state during the short 50 ms interval during which the images are collected. An equal number of triggers (20 in the specific case) and the successive 50 ms of data for each trigger, were taken.
5. The second run is done with the laser shot, that heat the foil every time the trigger is sent. Similarly to the first run, 20 shots and the successive 50 ms of data for each trigger, were taken.
6. The two runs are subtracted: the first to the second run. After that, each 50 ms interval of data is summed to the successive, for a total of 20 intervals. A sequence of 50 ms duration is finally obtained.

7. The sequence of IR images (50 images long) is submitted to the same data reduction described in the previous case.

4.4 Results without graphite coating on the laser side

The result is reported in Fig. 10. The value of thermal diffusivity around $1.60 \cdot 10^{-5}$ very close to that obtained in the previous case.

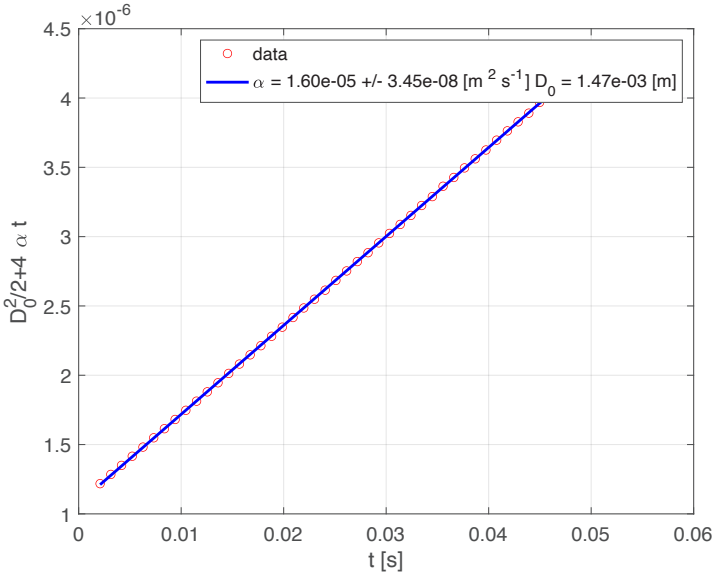

Figure 10. Plot of the diameter of the gaussian function that fit at best the temperature data. The fitting is applied to each image in sequence obtained after summing up 20 shots. The diameter Do at t = 0 s is related to the intercept of the line with the y axis.

5. Conclusion

In this work the thermal diffusivity of the AISI T302 thin foil was measured. The results are reported together with the in-plane testing procedure that use a pulsed laser spot as heat source and a fast IR camera to collect the temperature field.

References

[1] H. S. Carslaw and J. C. Jaeger. Conduction of Heat in Solids. Oxford University Press, second edition, 1959.

[2] Lord Kelvin William Thomson. Compendium of the Fourier mathematics for the conduction of heat in solids and the mathematically applied physical subjects of diffusion of fluids and transmission of electric signals through submarine cables. In Mathematical and Physical Papers, volume 2. Cambridge at the University press, 1884.

[3] F. Cernuschi, A. Russo, L. Lorenzoni, and A. Figari. In-plane thermal diffusivity evaluation by infrared thermography. Review of Scientific Instruments, 72(10):3988, 2001.

[4] C. Glorieux. Laser ultrasonics for material characterization and defect detection. https://www2.ung.si/~isschool/2018Erice/CG.pdf, 2018.